Experimental study of the near threshold $\pi^+p \to \pi^+\pi^+n$ cross section and chiral symmetry

M. E. Sevior,[1] A. Ambardar,[2] J. T. Brack,[2] P. Camerini,[5] F. Duncan,[2] J. Ernst,[3] A. Feltham,[9] N. Grion,[6] R. R. Johnson,[2] G. Koch,[2] O. Meirav,[7] D. F. Ottewell,[4] R. Rui,[5] G. R. Smith,[4] V. Sossi,[4] D. Theis,[3] and D. Vetterli[8]

[1] *University of Melbourne, Parkville, Victoria, 3052, Australia*
[2] *University of British Columbia, Vancouver, British Columbia, Canada V6T 2W5*
[3] *Universität Bonn, D-5300 Bonn 1, Germany*
[4] *TRIUMF, Vancouver, British Columbia, Canada V6T 2A6*
[5] *Dipartimento di Fisica dell'Universitá di Trieste, 34127 Trieste, Italy*
[6] *Istituto Nazionale di Fisica Nucleare, 34127 Trieste, Italy*
[7] *Elscint, Haifa, Israel*
[8] *Institute for Intermediate Physics, ETH-Hoenggerberg, 8093 Zuerich, Switzerland*
[9] *Institut fuer Experimental Physik, Klingelbergstr 82, CH-4052, Basel, Switzerland*

(Received 1 March 1993)

Total cross-section measurements of the $\pi^+p \to \pi^+\pi^+n$ reaction at pion kinetic energies of 180, 184, 190, and 200 MeV are reported. The threshold value for the amplitude $a(\pi^+\pi^+)$ as well as the s-wave, isospin 2, $\pi\pi$ scattering length a_2^0 were determined. The results were found to be in agreement with chiral perturbation theory and inconsistent with the calculations of Jacob and Scadron and the model of dominance by quark loop anomalies.

PACS number(s): 13.75.Gx, 11.30.Rd, 25.80.Ek

INTRODUCTION

Investigations of the underlying symmetries of quantum chromodynamics (QCD) have led to the belief that the chiral-symmetry-breaking formalism originally developed by Weinberg [1] is the low-energy manifestation of QCD [2]. Chiral perturbation theory (ChPT) extends the original Weinberg theory by including the effects of virtual meson loops in a perturbation expansion up to fourth order in meson energy. In general, the theory can be applied to systems involving light, strongly interacting mesons and nucleons. In the case of $\pi\pi$ scattering this is interpreted as including rescattering effects between interacting pions. There now exists a body of theoretical predictions with uncertainties substantially smaller than experimental errors for observables in simple, strongly interacting systems [2]. For the $\pi\pi$ system Gasser and Leutwyler [3] have made ChPT predictions for the s-wave, isospin 0, and isospin 2 scattering lengths, namely, $a_0^0 = (0.20 \pm 0.01)m_\pi^{-1}$, and $a_2^0 = (-0.042 \pm 0.002)m_\pi^{-1}$. In addition a number of other workers have made predictions for these scattering lengths. Jacob and Scadron [4] have calculated the effect of the f_0 meson resonance at $m_{\pi\pi} = 980$ MeV on the original Weinberg first-order calculations to predict $a_0^0 = 0.20m_\pi^{-1}$ and $a_2^0 = -0.028m_\pi^{-1}$. Lohse *et al.* [5] use a fit to higher-energy π data and a meson exchange model to obtain $a_0^0 = 0.31m_\pi^{-1}$ and $a_2^0 = -0.027m_\pi^{-1}$, and Ivanov and Troitskaya [6] have used the model of dominance by quark loop anomalies (QLAD), to predict $a_0^0 = 0.20m_\pi^{-1}$ and $a_2^0 = -0.060m_\pi^{-1}$. This model attributes $\pi\pi$ rescattering effects to σ exchange. A summary of these predictions is given in Table I. The predictions of Jacob and Scadron and of Ivanov and Troitskaya differ from ChPT only in the value for a_2^0.

Experimental data for a_2^0 are very sparse. The most precise value prior to this work was inferred from Roy equation fits by Froggatt and Petersen [7] to measurements at high energies and the data obtained from a measurement of the K_{e4} decay parameters by Rosselet *et al.* [8]. The value was found to be $a_2^0 = (-0.028 \pm 0.012)m_\pi^{-1}$ (a 43% uncertainty). This was a very indirect determination as it employed a combination of extrapolated results and dispersion relation constraints in the form of the Roy equations on the mostly isospin 0 data from the K_{e4} measurement. Near threshold, the angular momentum barrier limits the significant Feynman diagrams for

TABLE I. Predictions for the s-wave isospin 0 and 2 $\pi\pi$ scattering lengths.

Theory	$a_0^0(m_\pi^{-1})$	$a_2^0(m_\pi^{-1})$
Weinberg first order [1]	0.16	-0.045
CPT (Gasser and Leutwyler) [3]	0.20 ± 0.01	-0.042 ± 0.02
Jacob and Scadron [4]	0.20	-0.028
Meson exchange (Lohse *et al.*) [5]	0.31	-0.027
QLAD (Ivanov and Troitskaya) [6]	0.20	-0.060

the $\pi^+p \to \pi^+\pi^+n$ reaction to virtual $\pi\pi$ scattering and the contact interaction since these are the only large s-wave processes. As a result, at threshold the total cross section is determined by the s-wave isospin 2 scattering length a_2^0, and the contact interaction.

Olsson *et al.* [9] have derived the following relationship between a_2^0 and $a(\pi^+\pi^+)$ by means of an effective Lagrangian model which relates the total cross section at threshold to a_2^0 (with $f_\pi = 93.3$ MeV):

$$a(\pi^+\pi^+) = (-20.8a_2^0 + 0.242)m_\pi^{-1}, \quad (1)$$

where $a(\pi^+\pi^+)$ is the value of the amplitude at threshold for $\pi^+p \to \pi^+\pi^+n$ and is given by

$$\sigma = a(\pi^+\pi^+)^2 \times 1.28 \times 10^{-5} T^{*2} P_{\text{c.m.}}\ \mu\text{b}. \quad (2)$$

Here, T^* is the energy above threshold in the center of mass and $P_{\text{c.m.}}$ is the center-of-mass momentum of the incident pion. This equation contains $G^2_{\pi NN}$, the πNN coupling constant, and the number 1.28×10^{-5} is proportional to $G^2_{\pi NN}$. We used $G^2_{\pi NN} = 13.5$, which has been the accepted number for many years. Recently however this result has been challenged and values as low as $G^2_{\pi NN} = 12.9$ have been proposed [10]. Should a number this low become accepted as the correct value for $G^2_{\pi NN}$, the conclusions of this work would not be affected, although the actual numerical results for the matrix elements and scattering length would have to be adjusted by a few percent.

In this formalism the strength of the $\pi\pi$ interaction is characterized by the chiral-symmetry-breaking parameter ξ as derived by Olsson and Turner [9]. Then a_0^0 and a_2^0 can determined from ξ via the relations

$$a_0^0 = 0.0223(7 - \tfrac{5}{2}\xi)m_\pi^{-1}, \quad (3)$$

$$a_2^0 = -0.0223(2 + \xi)m_\pi^{-1} \quad (4)$$

with $f_\pi = 93.3$ MeV. When $\xi = 0$, the theory is equivalent to lowest-order ChPT. Olsson and Turner believed that a single value of ξ would determine a_0^0 and a_2^0 uniquely; however, they ignored the $\pi\pi$ rescattering effects incorporated at the one-loop level employed in the ChPT and QLAD approaches [3, 6]. Since $\pi\pi$ scattering in the $\pi^+p \to \pi^+\pi^+n$ reaction is purely isospin 2, one may use ξ as a phenomenological parameter to determine a_2^0. This is because both ξ and a_2^0 parametrize the strength of the $\pi\pi$ interaction, the only unknown amplitude of the $\pi^+p \to \pi^+\pi^+n$ reaction near threshold. Thus, within the framework of effective Lagrangians, the value of a_2^0 can be determined by fitting ξ to the measured cross sections.

A more detailed microscopic model of the $\pi^+p \to \pi^+\pi^+n$ reaction that includes the effects of Δ reaction mechanisms has been developed by Oset and Vicente-Vacas [11]. The authors confirm that the effects of Δ interactions are small below 200-MeV incident pion kinetic energy.

Recently, the OMICRON group published cross sections for $\pi^-p \to \pi^-\pi^0p$ and $\pi^+p \to \pi^+\pi^+n$ [12]. Near threshold, both these reactions are dominated by the isospin 2 amplitude. Their results are $a_2^0 = (-0.05 \pm 0.02)m_\pi^{-1}$ and $a_2^0 = (-0.08 \pm 0.01)m_\pi^{-1}$ for $\pi^-p \to \pi^-\pi^0p$ and $\pi^+p \to \pi^+\pi^+n$, respectively. The latter measurement is inconsistent with the K_{e4} result, which is almost a factor of 3 smaller. However if the OMICRON result of $a_2^0 = -0.08m_\pi^{-1}$ were confirmed it would be a major blow for ChPT, which predicts a value some 20 standard deviations closer to 0.

The aim of this experiment was to measure the total cross section for $\pi^+p \to \pi^+\pi^+n$ to a precision of 14% at energies where the effects of Δ interactions are small, i.e., at $T_\pi \leq 200$ MeV. The value of a_2^0 can be determined from the total cross sections by means of the aforementioned equations with an uncertainty of 7%. This precision will easily distinguish between the OMICRON and K_{e4} results. The results of this experiment were published in an earlier work [13]; in this publication we report the full experimental details of the measurement.

THE EXPERIMENT

The experiment was carried out on the $M11$ pion channel at TRIUMF and employed a novel technique. The experimental arrangement is shown in Fig. 1. Data were accumulated at incident pion energies of 200, 190, 184, 180, and 172 MeV. The latter energy was used to determine backgrounds since the laboratory energy threshold for $\pi^+p \to \pi^+\pi^+n$ is 172.3 MeV. The beam was defined by three, 2-mm-thick scintillators of cross-sectional di-

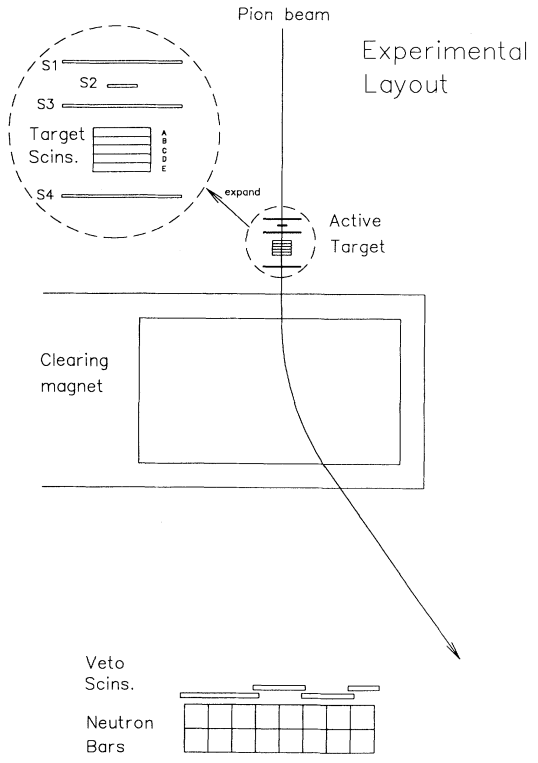

FIG. 1. The experimental arrangement. Pions from $M11$ are defined by the scintillators $S1$, $S2$, and $S3$. The scintillator target detects stopped positive pions by observing pion decay. Neutrons are detected in the scintillator array 2.6 m downstream of the target.

mensions 80×80 mm^2, 20×20 mm^2, and 80×80 mm^2, respectively, and coincidences between all three scintillators were counted as beam events. The dimensions of the small scintillator were chosen to define the beam spot well within the target. The large scintillators were designed to ensure that pions from preceding and following beam bursts were detected with high efficiency. The typical beam rate was 1.7 MHz and the momentum spread of the pion beam was $\pm 0.1\%$ of the central value. Protons were removed from the beam by means of a differential degrader, consisting of 1 in. of CH_2, placed at the dispersed focus midplane of the $M11$ channel. Any remaining protons were removed by pulse height cuts on the beam defining scintillators. Pions were distinguished from positrons by their time of flight through the $M11$ channel referenced to the primary proton pulses from the cyclotron. The positron contamination was typically 0.8% of the pion flux, which was corrected accordingly. It was not possible to determine the muon contamination this way; however, previous studies of the $M11$ channel [14] have established the muon flux to be 1.2% of the pion flux at the energies of this experiment and another correction of $1.2 \pm 1.2\%$ was applied to account for this contamination.

The target consisted of a set of 5 PILOT U plastic scintillators (chemical compound $CH_{1.1}$), each of dimensions $40 \times 40 \times 6$ mm^3 which were placed in a stack along the beam. Another $80 \times 80 \times 2$ mm^3 scintillator was located behind the target. It was used as a veto counter to define beam interactions in the target. The scintillator target was used to detect stopped $\pi^+ s$ from the $\pi^+ p \rightarrow \pi^+ \pi^+ n$ reaction. A large volume scintillator bar array was positioned 2.6 m downstream at 0° to detect the reaction neutrons. The array consisted of 16 bars each of dimensions $12.5 \times 10.0 \times 100.0$ cm^3 arranged as two vertical columns of 8 bars. The pion beam was swept away from the bars by a clearing magnet placed between the target and the array. In addition a set of four scintillators of 1.0 cm thickness were positioned immediately in front of the bars to veto stray charged particles from the target region.

The experimental setup exploited the restrictive kinematics of the $\pi^+ p \rightarrow \pi^+ \pi^+ n$ reaction near threshold to suppress background reactions such as $\pi^{+\,12}\mathrm{C} \rightarrow \pi^+ nX$. The kinematics of $\pi^+ p \rightarrow \pi^+ \pi^+ n$ require the reaction neutrons to be emitted into a narrow cone around 0° and to lie in the energy range 15–50 MeV. Thus the neutron bars placed at 0° intercepted a large fraction of the reaction neutrons while subtending less than 1% of the solid angle around the target.

Positive pions which stopped in the target were identified by a large prompt pulse from the π^+ energy loss, followed by a second pulse corresponding to the characteristic decay sequence $\pi^+ \rightarrow \mu^+ + \nu_\mu$. Three requirements were imposed to detect these signals from the scintillators. The first employed a custom built hardware circuit to detect the presence of two pulses closely spaced in time. Candidate events were detected in this circuit by differentiating the phototube output and passing the result through to a comparator. The threshold of the comparator was set to accept pulse heights characteristic of the monoenergetic pion decay muons. A separate circuit using standard NIM digital electronics detected the presence of two pulses within an 80-ns window. This circuit could detect muons which arrived as little as 7 ns after the prompt pulse. The second method used two charge integrating analogue-to-digital converters (ADC's) with different gate widths. One ADC was gated for a short time (15 ns) so that only the prompt pulse would appear within its integration period. The other was gated for a longer time (80 ns) so that the pion decay pulse could also be included. The difference between the normalized outputs showed the presence of a decay. The third and most powerful technique was to use a Tektronics 2440 digital oscilloscope as a 500 megasample per s transient digitizer. Signals from six different photomultipliers (the active target and the $S3$ scintillator) were time multiplexed into the two channels of the oscilloscope by means of Phillips Scientific 744 Linear Gates. Data from the oscilloscope were read out through the device's GPIB interface and into the general CAMAC data acquisition crate. The transient digitizer data were analyzed by fitting average phototube pulse shapes obtained from calibration runs to peak shapes recorded for each event. In this way, we determined the pulse height and time of both the prompt and delayed pulses. This technique provided unequivocal evidence for the presence of a pion decay pulse. The efficiency for detecting stopped pions was established from calibration runs during which low-energy positive pions from $M11$ were stopped in each segment of the active target. Figure 2 shows histograms for the height of the delayed pulse as determined from the transient digitizer data for typical calibration and data taking runs after correcting for an observed phototube aging effect. Figure 3 shows the transient digitizer data obtained from a candidate $\pi^+ p \rightarrow \pi^+ \pi^+ n$ event.

The trigger for data acquisition was a pion interaction in the target in coincidence with a neutron detected in the neutron bars, a second pulse detected with the hardware circuit and no other beam pion within 80 ns of the interaction event. Events containing two pions in one beam burst were vetoed by the $S4$ scintillator with 93% efficiency. The inefficiency came about because 7% of beam pions interacted in target. Since at most only 5% of beam bursts which contained at least one pion actually contained two, this inefficiency made a negligible impact on the beam normalization. These requirements together with the 43-ns time structure of the TRIUMF cyclotron limited the useful beam to only those beam events consisting of exactly one pion on target per proton pulse, preceded and followed by empty beam buckets. We determined the fraction of useful beam events from random samples of the pion beam and found it to be typically 80% of the flux as determined by the beam scalars, and the measured beam flux was corrected accordingly. The computer live time of the experiment was evaluated by separately counting the triggers presented to the data acquisition system and the triggers processed by the system. The ratio of the two numbers gave the relative live time of the experiment which was typically 85%.

The detection efficiency of the neutron bars was determined by stopping low-energy π^- particles in liquid

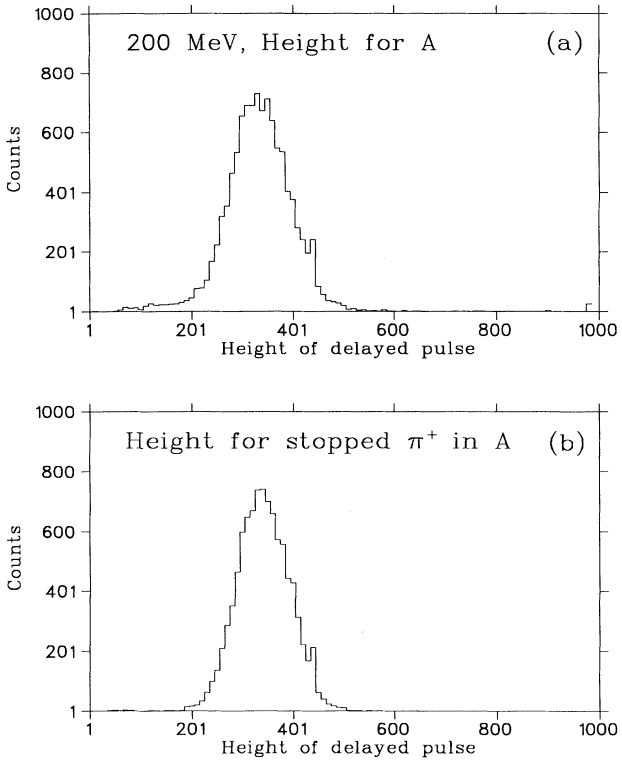

FIG. 2. Histograms of the delayed pulse heights due to muons from $\pi^+ \rightarrow \mu^+\nu$ decays from data taken at $T_\pi = 200$ MeV (a) and a calibration run (b). The pulse heights of the delayed muons were determined from the analysis of transient digitizer data.

deuterium and liquid hydrogen targets thus initiating the reactions $\pi^- d \rightarrow n + n$ and $\pi^- p \rightarrow \gamma + n$. These two reactions have well-measured branching ratios and therefore provide calibrated sources of monoenergetic neutrons (68 and 8.9 MeV) at energies above and below the neutron energy range of the threshold $\pi^+ p \rightarrow \pi^+\pi^+ n$ reaction. In addition, the 8.9-MeV neutrons provide useful pulse height information since the maximum energy the neutrons can deposit in the scintillator bars is from n-p elastic scattering which produces protons of up to 8.9 MeV. Because of quenching effects the light output from 8.9 protons is the same as 4.2-MeV electrons. Thus the leading edge of the pulse height histogram from 8.9-MeV neutrons provides a well-defined calibration point for the energy deposited in the neutron bars. With this calibration we determined the energy threshold of our neutron bars was 1.8 ± 0.1-MeV electron equivalent energy. We employed the Kent State neutron efficiency Monte Carlo code and these neutron bar thresholds to obtain the detection efficiency of the bars as a function of neutron energy. The estimated uncertainty in the efficiency was 10% as determined from the predictions of the Monte Carlo code at 8.9 and 68 MeV compared to the measured values. The effective neutron detection efficiency was established by convoluting the energy response of the neutron bars with the neutron energy distribution of the $\pi^+ p \rightarrow \pi^+\pi^+ n$ reaction. This weighted average neutron detection efficiency was $33 \pm 3\%$.

Another Monte Carlo (MC) code was used to determine the total acceptance of the experiment. Events were generated in accordance with the assumption that the reaction followed three-body phase space. This assumption is justified because the data were taken very close to threshold where s-wave processes dominate. The depth of the initial interaction in the target was weighted according to the variation of cross section across the energy thickness of the target. The code tracked the neutrons, pions, and decay muons from the reaction.

For neutrons the program traced the neutron to the plane of the neutron bars and recorded a hit if the neutron was inside the geometric acceptance of the array and in accordance with the detection efficiency of its energy. Thus the fraction of hits recorded in the MC code was directly proportional to the neutron detection efficiency and as stated above, gave an average neutron detection efficiency of $33 \pm 3\%$.

The charged particles from the reaction were tracked through the active target with step sizes such that the

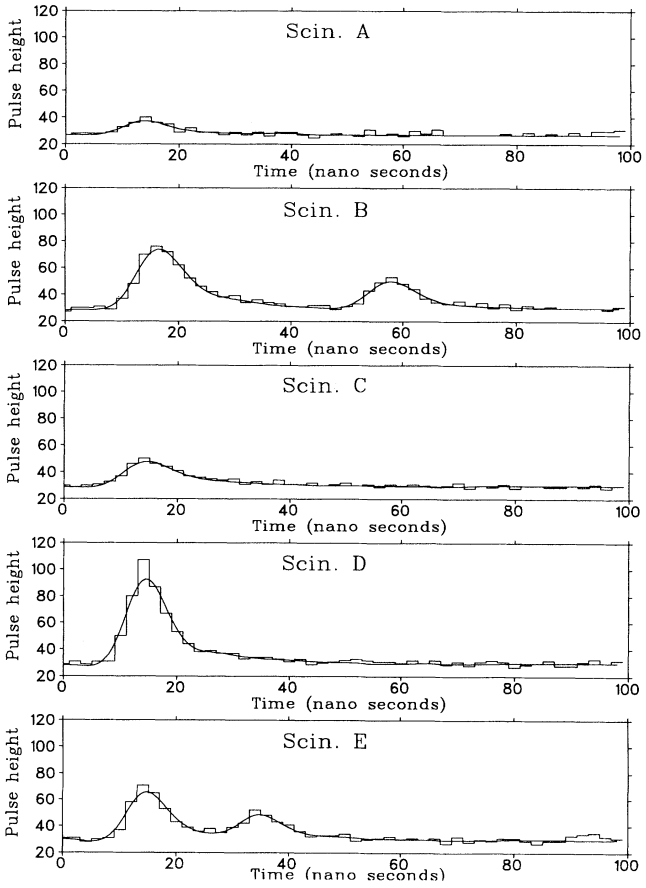

FIG. 3. Transient digitizer data from a typical event included in the "two-pion" analysis. In this event the incident pion has interacted in scintillator B. One pion from the interaction stops in scintillator B where it decays 40 ns later. The other pion traverses scintillators C and D then decays in scintillator E 20 ns later.

energy loss over a step was less than 10% of the particles kinetic energy except for particle's of 0.1 MeV or less. These particles were assumed to have zero range. The energy loss rate was calculated from the Bethe-Bloch equation and was set to the average of the energy loss before and after each step. If charged particles exited the scintillator they were assumed to be lost. The light output was calculated after each step using Birk's formula [15]:

$$\frac{dL(E)}{dE} = \frac{S}{1 + kB\frac{dE}{dx}} \tag{5}$$

with E the kinetic energy of the charged particle, L the light output of the scintillator, $\frac{dE}{dx}$ the energy loss as calculated by the Bethe-Bloch formula, S the normalization constant, and $kB = 0.0114$ cm/MeV as determined by Rozen *et al.* [16].

Formula (5) takes account of the light quenching effects near the end of a charged particle track. After the pions came to rest they were assumed to decay to 4.1-MeV muons at the rate given by the pion lifetime. The muons were emitted randomly into a 4π solid angle and also tracked through the scintillators until they stopped. The calculated light output was converted to the effective measured energy to establish the effect of the hardware double pulse detector thresholds on the stopped π^+ detection efficiency. As will be discussed later this detection efficiency varied with time because of the observed phototube aging effect. The fraction of the full 4π solid angle intercepted by our apparatus varied as a function of energy because of the kinematics of the $\pi^+p \to \pi^+\pi^+n$ reaction and was determined by our Monte Carlo acceptance code to be $18.1 \pm 0.4\%$, $35.6 \pm 0.8\%$, $58.2 \pm 0.3\%$, and $74.6 \pm 0.2\%$ at $T_\pi = 200$, 190, 184, and 180 MeV, respectively. The uncertainties quoted are the quadratic sum of errors from the uncertainty in the absolute energy of the incident beam (0.3 MeV) and the possible effects of a 2-mm misalignment between the active target and the beam defining scintillators. We believe this to be a conservative estimate since these devices were aligned with a theodolite to better than 0.5 mm.

The response of the active target was calibrated with events due to single passing pions, which deposit 1.25 MeV in each 6-mm scintillator as well as beam bursts containing two pions, giving 2.5 MeV. This enabled us to determine the effective energy thresholds of the hardware double pulse detector with an uncertainty of ± 0.1 MeV. These calibrations were made for each incident beam energy because a slow decay of the gain of the active target phototubes was observed over the course of the experiment. We attributed this decay to phototube aging due to high mean current operation. This surmise was verified in later bench tests when a similar decay in the output signal size was observed when the same make of phototube (Hammatsu R1535) was operated at gains and count rates similar to the experiment. As a result, the effective thresholds of the hardware detector increased over the course of the experiment, from typically 2.0 MeV to 2.6 MeV, which in turn decreased the stopped π^+ detection efficiency. The precision calibration, obtained for each energy, enabled us to account for this effect with our Monte Carlo acceptance code. In addition, another set of stopped π^+ detection efficiency calibrations were made at the end of the experiment. This second set of calibrations, when corrected for the increased effective hardware thresholds, were in good agreement with the original calibrations.

To analyze the data we added the energy deposited in the active target to the neutron energy, as determined by time of flight, to form the total kinetic energy sum ($T_{\rm sum}$) of the detected reaction products. $T_{\rm sum}$ is equal to $T_\pi^{\rm beam} - m_\pi - (m_n - m_p)$ for the $\pi^+p \to \pi^+\pi^+n$ reaction. The yield of the reaction was given by the peak area in the $T_{\rm sum}$ histogram less the background contribution.

Two techniques were used to extract yields from the raw data. The first required at least one pion to be detected in the active target. This trigger has a substantial background from $\pi^{+12}C \to \pi^+nX$ reactions which was suppressed by restricting the active target and neutron energies to the kinematic range allowed for the $\pi^+p \to \pi^+\pi^+n$ reaction. The remaining background was determined by a fit of the $T_{\rm sum}$ spectral shape of lower-energy runs (where the yield of $\pi^+p \to \pi^+\pi^+n$ was substantially less and different in $T_{\rm sum}$ than the run considered) to the regions in the $T_{\rm sum}$ histograms above and below the $\pi^+p \to \pi^+\pi^+n$ peak. For the 200-MeV data, the 184, 180, and 172 MeV runs were all used as backgrounds. For the 190-MeV data, the 180- and 172-MeV runs were used and the 184- and 180-MeV runs employed just the 172-MeV run as the background. Where more than one background was used, we found the extracted yields agreed within uncertainties (cf. Fig. 4). The foreground-to-background ratio for this technique was typically 1:4. We found yields from this "one-pion" analysis of 742 ± 100, 700 ± 90, 580 ± 70, and 160 ± 30 events at $T_\pi = 200$, 190, 184, and 180 MeV, respectively. The errors quoted are due to the estimated uncertainty in the background normalization. Because this trigger required the detection of at least one of two $\pi^+ \to \mu^+$ decays (i.e., there are two chances to detect one π^+), the efficiency of this trigger can be approximated by $\epsilon_t = 2\epsilon - \epsilon^2$, where ϵ_t is total trigger efficiency and ϵ is the efficiency of detecting a single π^+ decay. Since ϵ was typically 50%, $\epsilon_t = 75\%$. In practice each scintillator had a different efficiency because each employed a separate hardware π^+ detection circuit. Hence, this number should be viewed only as a qualitative guide. The total experimental acceptance varied as a function of energy because of the kinematics of the $\pi^+p \to \pi^+\pi^+n$ reaction and the decay of the gains of the phototubes. It was determined from the Monte Carlo code and, after including geometric effects as well as the neutron and stopped pion detection efficiencies, was found to be be $4.0 \pm 0.2\%$, $6.2 \pm 0.3\%$, $12.4 \pm 0.6\%$, and $13.2 \pm 0.7\%$ at $T_\pi = 200$, 190, 184, and 180 MeV, respectively. The uncertainties quoted reflect a possible target misalignment, the uncertainty in the stopped pion detection efficiency, and do not reflect the uncertainty in neutron detection efficiency.

The second analysis method required the identification of two π^+'s in two different scintillators. This extra requirement substantially reduced background events. The

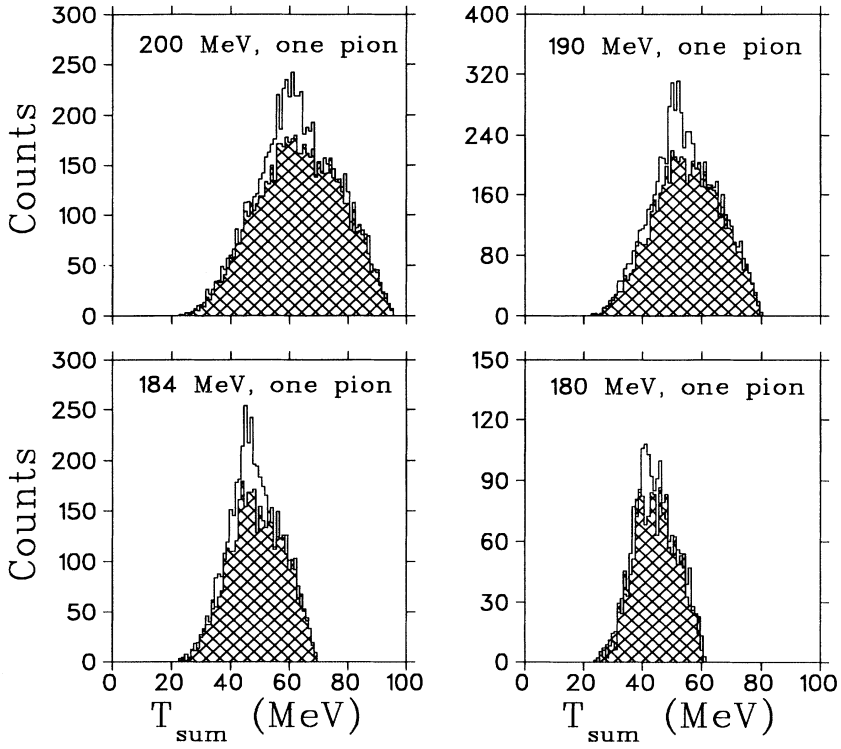

FIG. 4. The histograms for $T_{\rm sum}$ at T_π = 200, 190, 184, and 180 MeV for the one-pion technique with the neutron and target scintillator energies required to be in the allowed ranges for the $\pi^+p \rightarrow \pi^+\pi^+n$ reaction. Also shown superimposed as the hatched regions are background data from $\pi^{+12}{\rm C} \rightarrow \pi^+nX$ reactions that satisfy the same requirements.

signal-to-background ratio for this trigger was typically 10:1. This remaining background was due to events that contained two pions in one beam burst, both of which initiate $\pi^{+12}{\rm C} \rightarrow \pi^+nX$ reactions. The final yields from the "two-pion" analysis were obtained in a similar manner (cf. Fig. 5) by restricting the target scintillator and neutron energies to the kinematic range allowed for the $\pi^+p \rightarrow \pi^+\pi^+n$ reaction, then subtracting the background which was determined from the runs at lower energy. Once again the acceptance was determined from the Monte Carlo code and was found to be $0.69 \pm 0.07\%$, $0.57 \pm 0.06\%$, $1.58 \pm 0.16\%$, and $1.05 \pm 0.1\%$ at T_π = 200,

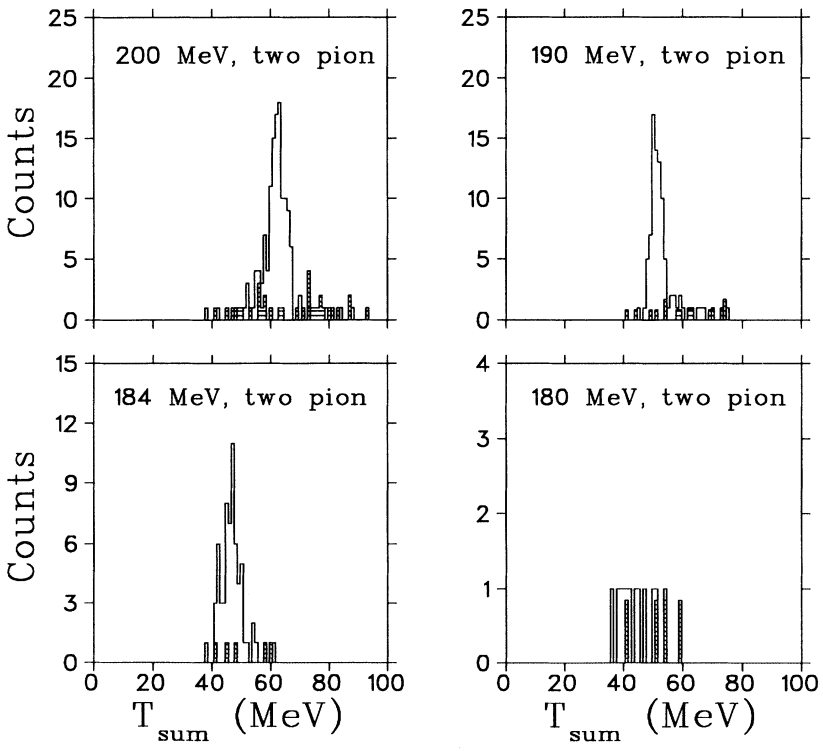

FIG. 5. The histograms for $T_{\rm sum}$ at T_π = 200, 190, 184, and 180 MeV for the two-pion technique with the neutron and target scintillator energies required to be in the allowed ranges for the $\pi^+p \rightarrow \pi^+\pi^+n$ reaction. Also shown superimposed as the hatched regions are background data that fulfill the same requirements.

190, 184, and 180 MeV, respectively. These acceptances are much smaller than for the one-pion analysis because the two-pion analysis required the detection of two pions in two different scintillators rather than having two chances to detect one pion in any scintillator. The transient digitizer data shown in Fig. 3 is from a typical two-pion event.

The two-pion analysis method gave us 124 ± 11, 74 ± 8, 65 ± 8, and 8 ± 3 events at $T_\pi = 200$, 190, 184, and 180 MeV, respectively. Figures 4 and 5 show histograms for $T_{\rm sum}$ at $T_\pi = 200$, 190, 184, and 184, obtained from both the one-pion and two-pion analysis methods, respectively, after restricting the target scintillator and neutron energies to the allowed kinematic ranges. Also shown superimposed are the background data for each energy and method of analysis.

The yield of the reaction is extremely sensitive to T_π since the total cross section is proportional to $P_{\rm c.m.} \times T^{*2}$. Consequently, care was taken to calibrate the central energy of the $M11$ beam line and to account for the decrease in yield as the beam lost energy through the target. The calibration was accomplished by determining the energy of ions (deuterons, tritons, ^{4}He) boiled off the production target by the proton beam and detected at the end of the $M11$ beam line with a surface barrier detector. We estimated the uncertainty in the $M11$ beam energy to be $\pm$ 0.3 MeV which corresponds to effective cross-section uncertainties of 2%, 4%, 6%, and 10% at 200, 190, 184, and 180 MeV, respectively. The cross section was corrected for the incident pion energy loss by assuming an underlying constant amplitude over the energy thickness of the target (6.25 MeV), and then integrating Eq. (2) over the energy thickness of the target at each bombarding energy. This provided an effective yield per incident pion which was used to normalize the cross section to its value at the incident beam energy.

RESULTS

The total cross sections and amplitudes for $\pi^+ p \to \pi^+\pi^+ n$ are listed in Table II and are displayed in Figs. 6 and 7. The data have been corrected for Coulomb interactions by means of the prescription given by Bjork *et al.* [17]. This increased the cross section by 5%, 7%, 8%, and 9% at 200, 190, 184, and 180 MeV, respectively. We found that the two analysis methods agree within their error bars which lends confidence to both the Monte Carlo acceptance calculations and the π^+ detection efficiencies. For example, an error of 10% in the π^+ detection efficiency results in a 7% shift in the final cross section from the one-pion analysis but a 23% change from the two-pion analysis. The systematic uncertainties associated with the measurement were neutron detection efficiency (10%), beam flux (2%), target thickness (3%), beam energy (2%, 4%, 6%, and 10% at 200, 190, 184, and 180 MeV, respectively), and experimental acceptance (5% and 10% for the one-pion and two-pion analysis methods, respectively). The experimental acceptance uncertainties include the uncertainties in the π^+ detection efficiency. The underlying amplitude shows no significant energy dependence, so the threshold value for $a(\pi^+\pi^+)$ can be obtained from a weighted average of the four values. We obtain $|\, a(\pi^+\pi^+) \,| \; (\pm \text{ stat} \pm \text{syst}) = (1.08 \pm 0.02 \pm 0.07) m_\pi^{-1}$ and hence $a_2^0 = (-0.040 \pm 0.001 \pm 0.003) m_\pi^{-1}$. We choose this root because the other leads to $a_2^0 = 0.063 m_\pi^{-1}$, in disagreement with phase shift analyses of $\pi^+ p \to \pi^+\pi^+ n$ at higher energies that show a_2^0 is negative [5]. We also fitted our cross-section data with the model of Oset and Vicente-Vacas by treating ξ as a free parameter. The result was a value of $\xi = -0.2 \pm 0.15$ (assuming $f_\pi = 93.3$ MeV) and so $a_2^0 = (-0.041 \pm 0.003) m_\pi^{-1}$. The uncertainty of 0.15 in ξ comes from the uncertainty in the overall normalization of the cross sections.

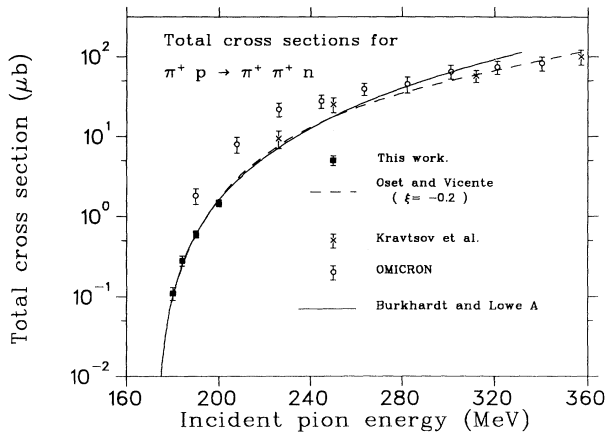

FIG. 6. Total cross sections as a function of pion bombarding energy are plotted for the $\pi^+ p \to \pi^+\pi^+ n$ reaction. The dashed line is the Oset–Vicente-Vacas calculation of the cross section with $\xi = -0.2$. The value of $\xi = -0.2$ was obtained from a fit to the data of the present experiment only. The solid line is the "unconstrained" fit of Burkhardt and Lowe to all $\pi p \to \pi\pi N$ data.

Figures 6 and 7 shows the extrapolated fit to our data

TABLE II. Total cross sections and amplitudes for $\pi^+ p \to \pi^+\pi^+ n$. The uncertainties quoted are the statistical and systematic errors, respectively.

T_π (MeV)	One pion (μb)	Two pion (μb)	Averaged (μb)	$a(\pi^+\pi^+)$ (m_π^{-1})
200	1.4±0.19 ±0.16	1.5±0.13±0.22	1.46±0.14±0.17	1.05±0.05±0.06
190	0.58±0.09±0.07	0.62±0.9±0.07	0.60±0.07±0.07	1.08±0.06±0.06
184	0.29±0.04±0.03	0.26±0.03±0.04	0.28±0.03±0.04	1.11±0.05±0.08
180	0.13±0.03±0.02	0.08 ±0.03±0.014	0.11±0.03±0.015	1.08±0.14±0.07

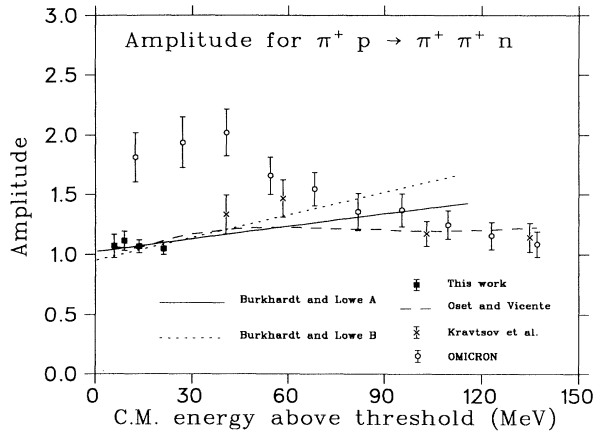

FIG. 7. Amplitudes for the $\pi^+ p \to \pi^+\pi^+ n$ reaction. The dashed line is the prediction of Oset and Vicente-Vacas with $\xi = -0.2$. The two fits of Burkhardt and Lowe are also shown. The solid line is the "unconstrained" fit. The dotted line is the "constrained" fit. The two different values of a_2^0 from the Burkhardt and Lowe analysis are reflected in the different values of their extrapolated fits to the amplitude at threshold.

is in good agreement with the results of Kravtsov *et al.* [18] obtained from the $\pi^- d \to \pi^-\pi^- pp$ reaction, and also with the data of OMICRON above 280 MeV. However the lower-energy data points of the OMICRON group are substantially larger than both the Kravtsov *et al.* data and our results. The lowest-energy OMICRON data point is a factor of 3 greater than the value expected from the other two measurements. This discrepancy is much larger than the assigned uncertainties of both experiments and leads to the exceptionally large value for a_2^0 reported by the OMICRON group. The consistency between the one-pion and two-pion analysis methods provides a tight check on the systematic uncertainties of the present measurement and supports our error assignments. Possible explanations of the discrepancy include the existence of an uncorrected background, incorrect assignment of the energy thresholds for the reaction pions, and/or a systematic error of the central beam energy in the OMICRON measurement. All effects would be largest at incoming pion energies near threshold.

Recently a global isospin analysis of all $\pi + p \to \pi\pi N$ measurements near threshold, including the results of this work, was performed by Burkhardt and Lowe [19]. They found good agreement between all channels of the reactions after the Kravtsov *et al.* and low-energy OMICRON $\pi^+ p \to \pi^+\pi^+ n$ results were removed from their database. Burkhardt and Lowe made two fits to the $\pi + p \to \pi\pi N$ data. In the first "unconstrained" fit only isospin invariance was assumed. This is shown as the solid line, "Burkhardt and Lowe *A*" in Fig. 7. For the second fit they also constrained a_0^0 and a_2^0 to satisfy the relation

$$\frac{a_2^0}{a_0^0} = \frac{\xi + 2}{2.5\xi - 7}$$

as derived by Olsson and Turner. This fit is shown as the dotted line, "Burkhardt and Lowe *B*" in Fig. 7. In this second, "constrained" fit an extra degree of model dependence is assumed since this equation is only valid within the model of Olsson and Turner and is not satisfied in other models such as the ChPT calculation of Gasser and Leutwyler. The unconstrained fit leads to $a_2^0 = (-0.037 \pm 0.004)$ $[(\xi = -0.4 \pm 0.2)m_\pi^{-1}]$ while the constrained fit gives $a_2^0 = (-0.032 \pm 0.004)m_\pi^{-1}$ $(\xi = -0.6 \pm 0.2)$. The unconstrained and more model-independent fit is in good agreement with our result, whereas the constrained fit, which includes $\pi - \pi$ isospin 0 data, agrees at the 2σ level. We take this result as further evidence of the validity of ChPT which predicts just such an effect. This is because the value of ξ needed to reproduce the isospin 0 result of ChPT is $\xi = -0.8$ while $\xi = -0.1$ is required to reproduce the isospin 2 prediction. The "constrained" fit allows just one value of ξ and favors the isospin 0 channels ($\pi^- p \to \pi^+\pi^- n$ and $\pi^0 p \to \pi^0\pi^0 n$) which have more data. Consequently, a more negative value of ξ was obtained from the constrained fit.

CONCLUSIONS

The Oset–Vicente-Vacas and the Olsson-Turner predictions for $a(\pi^+\pi^+)$ from a_2^0 both attribute 25% of the cross section to the contact term. However Oset and Vicente-Vacas include Δ reaction mechanisms which were not considered by Olsson and Turner. Since Oset and Vicente-Vacas predict small effects for these mechanisms at $T_\pi \leq 200$ MeV it is not surprising that the two models agree on the underlying value for a_2^0. It is worth noting that the calculations of Oset and Vicente-Vacas reproduce the data of Kravtsov *et al.* and the higher-energy OMICRON data, which was not included in the fit to obtain ξ, and indicates that the Δ reaction mechanisms are treated correctly.

To summarize, our data give a threshold value of $\mid a(\pi^+\pi^+) \mid = 1.08 \pm 0.02 \pm 0.07$ and, within the framework of effective Lagrangian models, imply a value for a_2^0 of $(-0.040 \pm 0.001 \pm 0.003)m_\pi^{-1}$. This value for a_2^0 is in agreement with Gasser and Leutwyler's prediction of -0.042 ± 0.002 and the K_{e4} measurement of -0.028 ± 0.012 and is inconsistent with the predictions of Jacob and Scadron $(-0.028m_\pi^{-1})$, the QLAD calculation of $-0.060m_\pi^{-1}$, and the OMICRON result of -0.08 ± 0.01.

ACKNOWLEDGMENTS

We would like to acknowledge Cam Marshall for his excellent operation of the liquid hydrogen and deuterium targets. We would also like to thank Juerg Gasser for many useful Bitnet conversations concerning chiral perturbation theory and Manolo Vicente-Vacas for making his effective Lagrangian code available to us. This work was made possible by grants from the Natural Sciences and Engineering Research Council of Canada and the German Bundesministerium für Forschung und Technologie.

[1] S. Weinberg, Phys. Rev. Lett. **17**, 616 (1966).
[2] J. Donoghue (unpublished); J. Gasser and H. Leutwyler, Phys. Rep. **87**, 77 (1982).
[3] J. Gasser and H. Leutwyler, Phys. Lett. **125B**, 321 (1983); **125B**, 325 (1983).
[4] R. J. Jacob and M. D. Scadron, Phys. Rev. D **25**, 3073 (1982).
[5] D. Lohse *et al.*, Nucl. Phys. **A516**, 513 (1990), and references within.
[6] A. N. Ivanov and N. I. Troitskaya, Yad. Fiz. **43**, 405 (1986) [Sov. J. Nucl. Phys. **43**, 260 (1986)].
[7] C. D. Froggatt and J. L. Petersen, Nucl. Phys. **B129**, 89 (1977); M. M. Nagels *et al.*, *ibid.* **B147**, 189 (1979).
[8] L. Rosselet *et al.*, Phys. Rev. D **15**, 574 (1977).
[9] M. G. Olsson and L. Turner, Phys. Rev. Lett. **20**, 1127 (1968); M. G. Olsson, E. T. Osypowski, and L. Turner, *ibid.* **38**, 296 (1977).
[10] R. A. Arndt *et al.*, Phys. Rev. Lett. **65**, 157 (1990).
[11] E. Oset and M. J. Vicente-Vacas, Nucl. Phys. **A446**, 584 (1985).
[12] G. Kernel *et al.*, Phys. Lett. B **225** 198 (1989); G. Kernel *et al.*, Z. Phys. C **48**, 201 (1990).
[13] M. E. Sevior *et al.*, Phys. Rev. Lett. **66**, 2569 (1991).
[14] G. Smith *et al.*, Phys. Rev. C **38**, 240 (1988).
[15] R. L. Craun and D. L. Smith, Nucl. Instrum. Methods **80**, 239 (1970).
[16] F. M. Rozen, N. Grion, and R. Rui, Nucl. Instrum. Methods A **267**, 101 (1988).
[17] C. W. Bjork *et al.*, Phys. Rev. Lett. **44**, 62 (1980).
[18] A. V. Kravtsov *et al.*, Nucl. Phys. **B134**, 413 (1978).
[19] H. Burkhardt and J. Lowe, Phys. Rev. Lett. **67**, 2622 (1991).